

A solvable generative model with a linear, one-step denoiser

Indranil Halder^{a,b}

^a*Harvard University, Cambridge, MA 02138*

^b*University of California, Davis, CA 95616*

ABSTRACT: We develop an analytically tractable single-step diffusion model based on a linear denoiser and present explicit formula for the Kullback-Leibler divergence between generated and sampling distribution, taken to be isotropic Gaussian, showing the effect of finite diffusion time and noise scale. Our study further reveals that the monotonic fall phase of Kullback-Leibler divergence begins when the training dataset size reaches the dimension of the data points. Along the way, we provide a mathematically precise definition of memorization to non-memorization transition when only finite number of data points are available. It is shown that the simplified model also features this transition during the monotonic fall phase of the aforementioned Kullback-Leibler divergence. For large-scale practical diffusion models, we explain why higher number of diffusion steps enhance production quality based on the theoretical arguments presented before. In addition, we show that higher diffusion steps does not necessarily help in reducing memorization. These two facts combined suggests existence of an optimal number of diffusion steps for finite number of training samples.

arXiv:2411.17807v2 [cs.LG] 23 Jan 2025

¹ihalder@g.harvard.edu

Contents

1	Introduction and summary of the results	1
1.1	Our contributions	2
1.2	Related works	3
2	Foundations of diffusion-driven generative models	3
3	A generative model based on a linear denoiser	4
3.1	Effect of finite diffusion time	5
3.2	Memorization to non-memorization transition	8
3.2.1	Mixing time-scale is optimal	8
3.2.2	Non-memorization is caused by the monotonic decay of generalization error	10
4	Non-linear diffusion model	12
5	Acknowledgements	15
A	Connection between ODE and SDE based generative models	18
B	Principle of deterministic equivalence	20
C	Generalization error from deterministic equivalence	22

1 Introduction and summary of the results

In recent years, generative artificial intelligence has made tremendous advancements - be it image, audio, video, or text domains—on an unprecedented scale. Diffusion models [1–3] are among the most successful frameworks, serving as the foundation for prominent content generation tools such as DALL-E [4], Stable Diffusion [5], Imagen [6], Sora [7] and numerous others. However, the factors that contribute to the strong generalization capabilities of diffusion models, as well as the conditions under which they perform optimally, remain open.

Ideally one would expect a trained diffusion model to produce images that are similar to the images it is trained on. But at the same time we don’t want the generated images to be too similar to the train dataset leading to memorization. Empirical observations show that for a small number of training samples, diffusion models memorize the training data [8, 9]. As the training dataset size increases,

they transition from memorizing data to a regime where it can generate similar looking new images [10]. Theoretically understanding this trade-off between production quality and non-memorization is a challenging task. Keeping this goal in mind, we introduce and study a linear denoiser based generative model that is analytically tractable and features some of the properties of realistic diffusion models. In particular our theoretical studies explain the effect of diffusion steps in production quality and generalization ability of the diffusion model.

1.1 Our contributions

Our main contributions to this paper are as follows:

1. We define a linear denoiser based generative model. Within the framework of the model, we present explicit formula for the Kullback-Leibler divergence between generated and sampling distribution, taken to be isotropic Gaussian, showing the effect of finite diffusion time and noise scale. In particular, our formula shows we can recover the sampling distribution from the generative model only if the noise scale is small enough compared to certain function of diffusion time.
2. We establish that aforementioned Kullback-Leibler divergence starts to decrease monotonically with addition of new training data when the size of the training set reaches the dimension of the data points as opposed to an exponential scale indicated by the curse of dimensionality.
3. Given a finite number of samples from a probability distribution, the true distribution can be approximated by a L^2 -distance optimal Gaussian kernel. We observe that in the context of higher dimensional statistics, the variance of the kernel coincides with the mixing time for the samples under Ornstein-Uhlenbeck forward diffusion process.
4. Using this observation, we formulate a mathematically precise metric for calculating pairwise distance between generated, sampling and train distribution when only finite amount of data is available and give a definition of the memorization to non-memorization transition.
5. We show that the linear denoiser based model features a transition from memorization to non-memorization during monotonic decrease of Kullback-Leibler divergence between generated and sampling distribution.
6. Our metric allows us to systematically study the generalization properties of a realistic diffusion model. Using this on Gaussian mixture model training set, we quantify the fact that larger diffusion steps leads to better production quality. On the other hand, we argue that the theorem that we proved before gives

us theoretical explanation of this fact. This also tells us how to scale noise introduced in the diffusion process with diffusion time for good production quality.

7. Motivated by the results of linear denoiser based model, we hypothesize that memorization-to-non-memorization transition is caused by the decay of generalization error for generic diffusion models. For realistic diffusion models we show that this result holds. Furthermore we show that higher diffusion steps does not necessarily reduce memorization of diffusion models. Combining this with the point mentioned above, it tells us that given finite amount of training data, there exists an optimal number of diffusion steps.

1.2 Related works

The idea of diffusion-based generative models originated in the pioneering work of [1–3, 11, 12]. The quality of the generated images was further enhanced through guided diffusion at the cost of reduced diversity [13–17]. Also, empirical observations have indicated that increasing diffusion steps leads to more visually appealing images [18]. In this work we present theoretical understanding of this observation.

In a compelling study, [10] has demonstrated that as the train dataset size increases diffusion models make a transition from memorizing the train dataset of facial images to a non-memorization regime where two diffusion models of identical architecture can produce similar-looking new faces even when trained on disjoint sampling sets. [19] has given a precise definition of the memorization capacity of a diffusion model. Recent works of [20–22] has pointed out how diffusion models can combine local features to generate new images. However when the model is not memorizing, to what extent it is actually generalizing and sampling from the underlying distribution is an open question that we study in this paper.

2 Foundations of diffusion-driven generative models

In the domain of image generation, we don't know the exact functional form of the sampling distribution $\rho(x)$. However we have access to a finite number of samples from it and the goal is to generate more data points from the unknown probability density $\rho(x)$. Traditional likelihood maximization techniques would assume a trial density function ρ_θ and try to adjust θ so that likelihood for obtaining known samples is maximized. In this process determination of the normalization of ρ_θ is computationally expensive as it requires multi-dimensional integration (typically it is required for each step of the optimization procedure for θ). Diffusion based generative models are an alternative [1–3]. In this section, we review basic notions of these stochastic differential equation based models. In particular, we examine an exactly solvable

stochastic differential equation (SDE). The Itô SDE under consideration is known as the Ornstein-Uhlenbeck Langevin dynamics and is expressed by:

$$dX_t^F = -X_t^F dt + \sqrt{2}dW_t, \quad X_t^F \sim \rho(t). \quad (2.1)$$

The score function associated with the stochastic process will be denoted as (see Appendix A for details of notation and conventions)

$$s(t, x) = \nabla_x \log \rho(t, x) = \frac{1}{\rho(t, x)} \nabla_x \rho(t, x) \quad (2.2)$$

The probability density ρ satisfies the transport equation (see (A.3) in Appendix A)

$$\begin{aligned} \partial_t \rho(t, x) &= \nabla \cdot ((x + s(t, x))\rho(t, x)) \\ &= \nabla^2 \rho(t, x) + x \cdot \nabla \rho(t, x) + d\rho(t, x). \end{aligned} \quad (2.3)$$

The dimension of the data is defined to be given by $d = \dim(x)$. The time evolution of the probability distribution is exactly solvable and given by

$$\rho(t, X_t^F) = \int dX_0^F \rho(0, X_0^F) \mathcal{N}(X_t^F | X_0^F e^{-t}, 1 - e^{-2t}). \quad (2.4)$$

Suppose we know the probability density $\rho(0, x)$ exactly. One way to sample from it would be to use the knowledge of the exact score function $s(t, x)$ in the reverse diffusion process (see (A.10) in Appendix A), i.e.,

$$dX_t^B = (-X_t^B - 2s(t, X_t^B))dt - \sqrt{2}dW_{1-t} \quad (2.5)$$

starting from a late time distribution $\rho(T, x)$ (it is assumed that we know how to sample from $\rho(T, x)$).

This method requires estimating the score function s from known samples - it can be obtained by minimizing Fisher divergence [23] (see (A.8) in Appendix A for more details) using techniques such as the kernel method [24] or denoising score matching [25].

3 A generative model based on a linear denoiser

In this section, we define and study a linear denoiser based generative model which is analogous to a one step diffusion model. Before explaining the model, we note certain basic facts about the diffusion process based on a finite number of samples. Given n samples $\rho(x)$ can be approximated by the Dirac delta distribution $\hat{\rho}(0, x) \equiv \frac{1}{n} \sum_{k=1}^n \delta(x - x_k), x \in \mathbb{R}^d$. The time evolution of the probability distribution under Ornstein-Uhlenbeck diffusion process can be obtained from (2.4)

$$\hat{\rho}(t, x) = \frac{1}{n} \sum_{k=1}^n \mathcal{N}(x | x_k e^{-t}, 1 - e^{-2t}) \quad (3.1)$$

This motivates us to sample $Y_k, k = 1, 2, \dots, n$ from the underlying distribution $\rho(x)$ and add noise $Z_k \sim \mathcal{N}(0, \mathbf{I}_d)$ to it to obtain noisy samples $X_k = e^{-T}Y_k + \sqrt{\Delta_T}Z_k, \Delta_T = \lambda\delta_T = \lambda(1 - e^{-2T})$. Here T is the diffusion time cut-off and λ is a free hyperparameter that controls the amount of noise added¹. For simplicity, we add the entire noise in one step in contrast to the multi-step process of realistic diffusion models.

The denoiser based model, trained on the data above, as input takes a noisy sample X and generates a clean sample Y . In this paper, we consider a linear model $Y = \hat{\theta}_0 + \hat{\theta}_1 X$ as prototype denoiser for analytical tractability. The parameters $\hat{\theta}_0, \hat{\theta}_1$ are solution to the linear regression problem of predicting $\{Y_k\}$ given $\{X_k\}$ and given by²

$$\begin{aligned}\hat{\theta}_1^T &= (x^T x)^{-1} x^T y, \quad \hat{\theta}_0 = \hat{Y} - \hat{\theta}_1 \hat{X} \\ \hat{X} &= \frac{1}{n} \sum_{k=1}^n X_k, \quad \hat{Y} = \frac{1}{n} \sum_{k=1}^n Y_k\end{aligned}\tag{3.2}$$

Here x, y are $n \times d$ dimensional matrices whose k -th row is $(X_k - \hat{X})^T, (Y_k - \hat{Y})^T$ respectively.

To generate samples from the trained diffusion model we first draw X from $\mathcal{N}(\mu_X, \sigma_X^2 \mathbf{I}_d)$, motivated by the fact that late time distribution can be reliably approximated by a Gaussian distribution with

$$\mu_X = e^{-T} \hat{Y}, \quad \sigma_X^2 = e^{-2T} \frac{1}{nd} \sum_{k=1}^n |Y_k - \hat{Y}|^2 + \Delta_T\tag{3.3}$$

and then use the diffusion model to predict corresponding $Y = \hat{\theta}_0 + \hat{\theta}_1 X$. The generated probability distribution for a given set $\{(X_k, Y_k), k = 1, 2, \dots, n\}$ is

$$\rho_G(Y | \{(X_k, Y_k)\}) = \mathcal{N}(Y | \hat{\theta}_0 + \hat{\theta}_1 \mu_X, \sigma_X^2 \hat{\theta}_1^T \hat{\theta}_1)\tag{3.4}$$

The generated probability distribution as defined above is a random variable conditioned on $\{(X_k, Y_k), k = 1, 2, \dots, n\}$ which itself is a random variable. We consider its expectation value $\rho_G(Y)$ by further sampling $Y_k \sim \rho$ and $X_k = e^{-T}Y_k + \sqrt{\Delta_T}Z_k$ as mentioned above.

3.1 Effect of finite diffusion time

In this subsection, we study the effect of finite diffusion time T and noise scale λ on generalization error for the linear diffusion model defined above. We restrict our discussion to sampling from isotropic Gaussian distribution $\rho = \mathcal{N}(\mu, \sigma^2 \mathbf{I}_d)$. The distance between the underlying distribution ρ and the generated ρ_G distribution from the diffusion model as given in (3.4) can be measured in terms of Kullback–Leibler

¹This corresponds to scaling the noise term in (2.1) by a factor of $\sqrt{\lambda}$.

²A natural generalization of this is to feature kernel regression instead of linear regression.

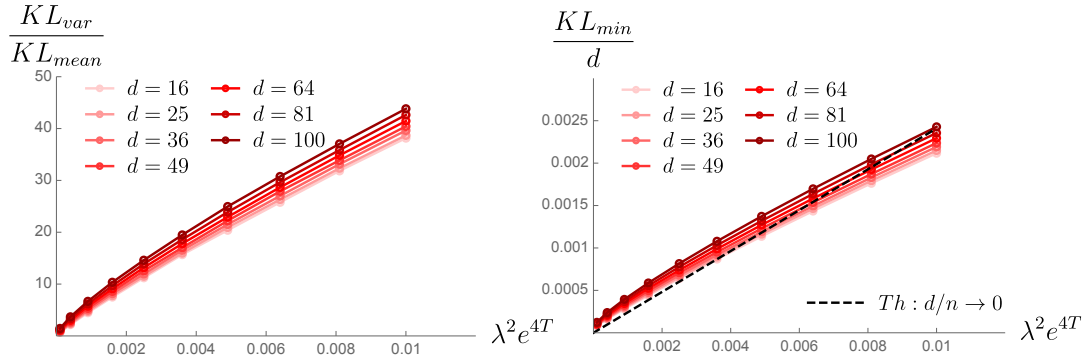


Figure 1: We plot various contributions to KL divergence between the generated data from the linear denoiser based generative model and sampling distribution taken to be an isotropic Gaussian of mean $\mu = 10$ and diagonal standard deviation $\sigma = 1$ of dimension d . We have fixed the diffusion time cut-off $T = 2$ and varied the noise scale $\lambda = \hat{\lambda}e^{-4}$. The train dataset size $n = 10^4$ is taken to be much bigger compared to the dimension d . From the plot on left we see there exists a regime of parameters when $KL_{mean} \ll KL_{var}$. This justifies our assumption of ignoring KL_{mean} in analytic calculation presented in appendix C. The plot on the right compares the numerical results against the theoretical result and shows that the minimum KL divergence attainable in $d/n \rightarrow 0$ limit scales quadratically with the noise parameter $\hat{\lambda} = \lambda e^{2T}/\sigma^2$ for small values of the later.

divergence. Further it can be decomposed as $KL(\rho||\rho_G) = KL_{mean} + KL_{var} \geq KL_{var}$. Where the contributions KL_{mean}, KL_{var} are related to the difference between generated and the underlyingly distribution in mean and variance

$$\begin{aligned}
 KL_{mean}(\rho_G|\rho) &= \frac{1}{2\sigma^2}(\mu - \hat{\mu}_G)^T(\mu - \hat{\mu}_G) \\
 KL_{var}(\rho_G|\rho) &= \frac{1}{4}\text{Tr} \left(\left(\frac{\hat{\Sigma}_G}{\sigma^2} - I \right)^2 \right) \\
 \hat{\mu}_G &= \hat{\theta}_0 + \hat{\theta}_1 \mu_X, \quad \hat{\Sigma}_G = \sigma_X^2 \hat{\theta}_1^T \hat{\theta}_1
 \end{aligned} \tag{3.5}$$

The inequality follows because KL_{mean} is a positive semi-definite quantity. We numerically show in figure 1 that there exists a regime of small λ where $KL_{mean} \ll KL_{var}$ making the inequality above an approximate equality. We will see that small λ regime leads to smaller value of KL_{var} and we are interested in studying how small λ has to be for a given value of T for recovering the underlying sampling distribution. Keeping this goal in mind, in Appendix C we provide theoretical analysis proving the following theorem in this domain.

Theorem 3.1. *When the linear diffusion model described above is trained on n samples from isotropic Gaussian distribution $\rho = \mathcal{N}(\mu, \sigma^2 \mathbf{I}_d)$ in the limit of $n \rightarrow \infty$ holding $\alpha = d/n$ fixed, following lower bound on the KL divergence between generated and sampling distribution holds $KL(\rho||\rho_G) \geq KL_{var}$. If further we restrict ourselves to small noise scale $\lambda = \hat{\lambda}\sigma^2 e^{-2T}$, $\hat{\lambda} \ll 1$, then an explicit expression for the statistical expectation value of KL_{var} can be obtained order by order in $\hat{\lambda}$ based on the theory of deterministic equivalence. More specifically for $\alpha < 1$ we have*

$$\begin{aligned} \langle KL_{var} \rangle &= \frac{d\alpha\hat{\lambda}e^{-4T}(e^{2T}-1)}{2(1-\alpha)} + \frac{d\hat{\lambda}^2e^{-8T}(e^{2T}-1)^2}{4(1-\alpha)^3} \\ &\times (\alpha^2 + (1-\alpha)^3e^{4T} + 4\alpha(1-\alpha)^2e^{2T}) + \mathcal{O}(\hat{\lambda}^3) \end{aligned} \quad (3.6)$$

and for $\alpha > 1$

$$\begin{aligned} \langle KL_{var} \rangle &= d\frac{\alpha-1}{4\alpha} + \frac{d\hat{\lambda}e^{-4T}(e^{2T}-1)}{2(\alpha-1)} \\ &+ \frac{d\hat{\lambda}^2e^{-8T}(e^{2T}-1)^2}{4(\alpha-1)^3\alpha} (\alpha^3 + (\alpha-1)^3e^{4T}) \\ &+ 4\alpha(\alpha-1)^2e^{2T} + \mathcal{O}(\hat{\lambda}^3) \end{aligned} \quad (3.7)$$

A detailed proof of the theorem is available in appendix C. In the appendix, we also provide general formula with a ridge parameter. The expression with the ridge parameter is fairly complicated and in the main text we study only the ridgless version of it.

Lemma 3.2. *For $n > d$, KL_{var} is a monotonically decreasing function of n/d .*

This fact can be easily seen from the plot on the right in figure 2. The theorem shows that as we approach $\alpha = 1$, KL_{var} becomes unbounded from above, verified by experimental analysis in figure 2. In the domain of $\alpha > 1$, we see from the theorem above that KL_{var} is no longer monotonic, for instance the first term is increasing and second term is a decreasing contribution. This fact is also seen in figure 2. We conclude that KL divergence between generated and sampling distribution decreases monotonically with addition of more training points for $n > d$.

Lemma 3.3. *In $n/d \rightarrow \infty$ limit, KL_{var}/d scales as $\lambda^2 e^{4T}(1 - e^{-2T})^2$. Hence we conclude we can recover the underlying sampling distribution in this limit only if $\lambda e^{2T}(1 - e^{-2T}) \ll 1$.*

This is in agreement with the plot on the right in figure 1. Intuitively this fact can be understood as follows. Noisy samples are obtained from clean ones from $X_k = e^{-T}Y_k + \sqrt{\lambda(1 - e^{-2T})}Z_k$. Hence we can distinguish the data of the clean samples from noise only if $e^{-T} \gg \sqrt{\lambda(1 - e^{-2T})}$.

So far we have stated our results in terms of KL divergence, however qualitative facts that we learned remain valid for other measures of distance as well. To show this we have plotted the Hellinger distance between the sampling and generated distribution in figure 3 based on expectation value of the following expression

$$\begin{aligned}
& \mathbb{H}^2(\rho || \rho_G | \{(X_k, Y_k), k = 1, 2, \dots, n\}) \\
&= \frac{1}{2} \int dx (\sqrt{\rho(x)} - \sqrt{\rho_G(x)})^2 \\
&= 1 - \left(\frac{2^d \sqrt{\det(2\pi\sigma_X^2 \hat{\theta}_1^T \hat{\theta}_1) \det(2\pi\sigma^2 \mathbf{I}_d)}}{\det(2\pi(\sigma_X^2 \hat{\theta}_1^T \hat{\theta}_1 + \sigma^2 \mathbf{I}_d))} \right)^{\frac{1}{2}} \\
&\quad \times e^{-\frac{1}{4}(\hat{\theta}_0 + \hat{\theta}_1 \mu_X - \mu)^T (\hat{\theta}_1^T \hat{\theta}_1 + \sigma^2 \mathbf{I}_d)^{-1} (\hat{\theta}_0 + \hat{\theta}_1 \mu_X - \mu)}
\end{aligned} \tag{3.8}$$

The smaller the value of H^2 the closer the generated distribution is to the original one. We see from the plot that Hellinger distance decreases with higher slope for $n > d$.

3.2 Memorization to non-memorization transition

In this subsection, we define and analyze a precise metric for memorization to non-memorization transition of the linear denoiser based generative model when only finite number of samples are available from the sampling distribution ρ . This collection of samples will be called the original dataset and we will train the diffusion model on a subset of it. To this end we need to precisely define pairwise distance between training, generated and original dataset. This is achieved by observing that mixing time-scale is optimal, we explain this point next and later study memorization to non-memorization transition.

3.2.1 Mixing time-scale is optimal

In this subsection, we present our observation: given n samples from a distribution $\rho(x)$, the mixing time t_M —defined as the minimum diffusion time after which two points exert significant mutual influence—corresponds to the optimal variance of a non-parametric Gaussian density estimator. We now proceed to explain this point in detail.

To formalize the definition of t_M we consider $x = x_1 e^{-t} + \sqrt{\delta_t} Z$ for some $Z \sim \mathcal{N}(0, \mathbf{I}_d)$ and decompose $\hat{\rho}(t, x)$ into two parts $\hat{\rho}(t, x) = Z_1 + Z_{1^c}$, with

$$\begin{aligned}
Z_1 &= \frac{1}{n} \mathcal{N}(x | x_1 e^{-t}, 1 - e^{-2t}) \\
Z_{1^c} &= \frac{1}{n} \sum_{k=2}^n \mathcal{N}(x | x_k e^{-t}, 1 - e^{-2t})
\end{aligned} \tag{3.9}$$

It can be shown that in the limit $n \rightarrow \infty$ with $\log n/d$ fixed, Z_{1^c} is an increasing function of t such that for $t < t_M$, $Z_{1^c} < Z_1$ and at mixing time $t = t_M$, $Z_1 =$

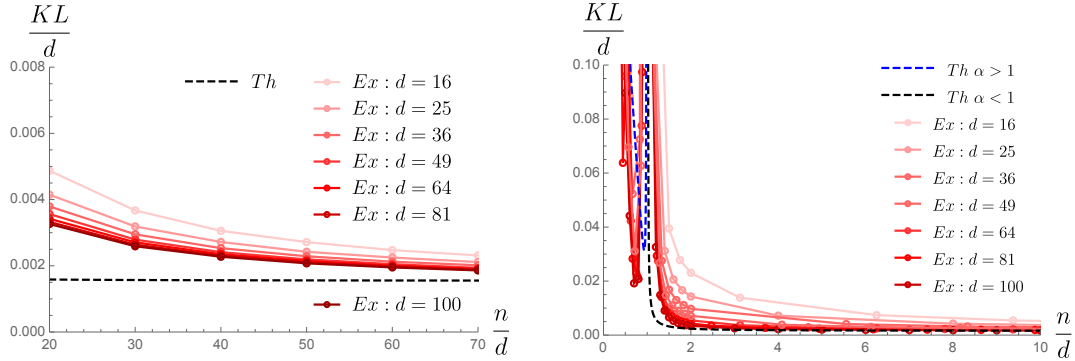


Figure 2: The data set is the same as in Fig. 1. We have fixed the diffusion time to be $T = 2$ with noise scale $\lambda = 0.8e^{-4}$. On the left, we plot KL divergence between the generated and sampling distribution after truncation to the quadratic order in λ , as given in (C.10), in the regime of small d/n comparing experimental data (in red) and theoretical result for the lower bound as given in (3.6) (in black). The numerical results on the right plot shows that KL divergence between the generated and underlying distribution scales as d times solely a function of $\alpha = d/n$ without additional n, d dependence as we take n, d large keeping their ratio fixed. This fact is analytically established in (3.6),(3.7) and the analytical expression is plotted in black for $\alpha < 1$ and blue $\alpha > 1$. We see that KL divergence monotonically decreases with addition of more training samples for $n > d$ and becomes unbounded at $n = d$. Beyond this for $n < d$, KL divergence is not a monotonic function of d/n .

Z_{1c} . When $\rho(0, x) = \mathcal{N}(x|\mu, \sigma^2 \mathbf{I}_d)$, one can explicitly calculate t_M using ideas from random energy model [26] to be given by [27]

$$t_M = \frac{1}{2} \log \left(1 + \frac{\sigma^2}{n^{\frac{2}{d}} - 1} \right) = \frac{1}{2} \left(\frac{\sigma}{n^{\frac{1}{d}}} \right)^2 + \mathcal{O} \left(\frac{\sigma^4}{n^{\frac{4}{d}}} \right) \quad (3.10)$$

In the second equality, we have further expanded the expression above in the limit $\log n/d \gg \log(\sigma)$ and kept only the leading order term.

On a separate line of work, [28–30] has minimized the expectation value of $\int dx (\rho(x) - \rho_E(x))^2$, $\rho_E = \frac{1}{n} \sum_{k=1}^n \mathcal{N}(x|x_k, \epsilon^2)$ over ϵ for large n at fixed d to obtain the following formula for the optimal ϵ

$$\epsilon = \left(\frac{4}{d+2} \right)^{\frac{1}{d+4}} \frac{\sigma}{n^{\frac{1}{d+4}}} = \frac{\sigma}{n^{\frac{1}{d}}} + \mathcal{O} \left(\frac{\log n}{d^2} \right) \quad (3.11)$$

To go to the second equality we have taken d large. The error term above suggests leading order term is a good approximation only when $\log n/d \ll d$. On the other

since the calculation is done first keeping d fixed and then taking n large we must have $\log n/d \gg 1$.

We observe that the first term in (3.11) matches precisely with the expression of $\sqrt{2t_M}$ as calculated above in (3.10). This shows that the region when both the analytical formula for mixing time of diffusion process t_M and that of the optimal standard deviation of the Gaussian kernel ϵ is valid, they coincide with each other and $\hat{\rho}(t_M, x)$ coincides with $\rho_E(x)$ to the leading order in small ϵ .

The discussion above is valid for large n, d . However it serves as motivation for the following definition valid for generic dataset.

Definition 3.4. Given access to only N data-points from the sampling distribution $\rho(x)$, original probability distribution is defined to be given by

$$\rho_O(x) \equiv \frac{1}{N} \sum_{k=1}^N \mathcal{N}\left(x|x_k, \frac{\hat{\Sigma}_O}{N^{\frac{2}{d}}}\right) \quad (3.12)$$

Where $\hat{\Sigma}_O$ is the covariance inferred from N data points. For a sub-set of $n \leq N$ data-points we further define the train distribution to be

$$\rho_T(x) \equiv \frac{1}{n} \sum_{k=1}^n \mathcal{N}\left(x|x_k, \frac{\hat{\Sigma}_O}{n^{\frac{2}{d}}}\right) \quad (3.13)$$

3.2.2 Non-memorization is caused by the monotonic decay of generalization error

Armed with the definitions (3.13), (3.12) given in previous section, we define pairwise distances $E_{TG} = \int dx (\rho_T(x) - \rho_G(x))^2$, $E_{OG} = \int dx (\rho_O(x) - \rho_G(x))^2$ between probability distributions ρ_O, ρ_T, ρ_G .³

Definition 3.5. The denoiser based model is said to be *memorizing* the training data when the probability that the relative distance $\Delta = E_{TG} - E_{OG} > 0$, i.e., $P(\Delta > 0)$, is smaller than unity. Conversely, the model is in the *non-memorization regime* when $P(\Delta > 0) = 1$.

Clearly when $P(\Delta > 0)$ is near to unity the generated data is far from the training dataset compared to the original dataset, justifying our definition above. The analog of E_{TG} has been appeared in previous work on the subject [19], however

³Another possibility is to consider the Wasserstein distance. The simplest version of the Wasserstein distance between the original and generated dataset would require generating N samples from the diffusion model and then N^3 order computations to find the optimal permutation of the points for computing the distance. This is an extremely computationally expensive technique and we would not pursue it in this paper.

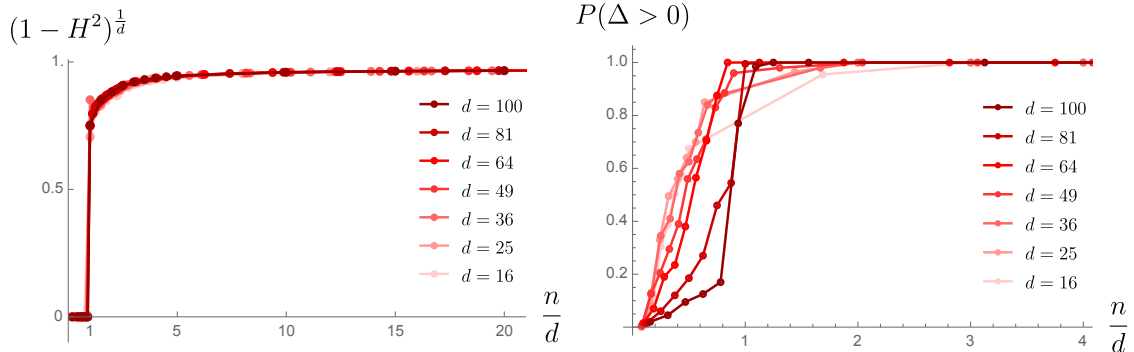


Figure 3: The data distribution is same as in Fig. 2. For the linear denoiser based generative model we set $T = 2, \lambda = e^{-4}$. The plot on the left is based on the expression of H^2 for the model in (3.8). The plot establishes that the decay in Hellinger distance begins at $n = d$ as opposed to $n = \mathcal{O}(e^d)$. The plot on the right is based on the expression in (3.14) and (3.15). The original dataset is composed of $N = 10^4$ samples. We de-singularized the train and the original distribution according to our definition in (3.13) and (3.12). We notice that the model stops memorizing at $n = \mathcal{O}(d)$. Comparing with the plot on the left, we conclude that the model stops memorizing when the Hellinger distance between the sampling and generated distribution starts to decrease.

to the best of our knowledge the study of E_{OG} when only finite number of data points are available in the original distribution is our contribution.

We expect that as the size of the training dataset is increased the model makes a transition from memorization to non-memorization regime. We will show that this is the case next. Before we proceed, note that during this transition Δ changes from most likely being negative to being most likely being positive. This change in relative distance Δ is one condition on two individual distances E_{OG}, E_{TG} . Therefore on the onset on this transition the behavior of E_{OG}, E_{TG} are not constrained completely. For instance, mathematically it is possible that on the on-set of the transition memorization performance degrades marking increase in E_{TG} whereas the generalization performance, governed by E_{OG} , does not improve. We will soon see that this is not what happens in the linear diffusion model. In fact, we will show that the memorization to non-memorization transition is due to a fall phase of the Hellinger distance between the generated and sampling distribution. To calculate these quantities for

the linear diffusion model we use following expressions

$$\begin{aligned}
& E_{TG}(\{(X_k, Y_k), k = 1, 2, \dots, n\}) \\
&= \frac{1}{\sqrt{\det(4\pi\hat{\theta}_1^T\hat{\theta}_1\sigma_X^2)}} - 2 \sum_{k=1}^n \frac{e^{-\frac{1}{2}(\hat{\theta}_0+\hat{\theta}_1\mu_X-Y_k)^T(\hat{\theta}_1^T\hat{\theta}_1\sigma_X^2+\epsilon_T^2)^{-1}(\hat{\theta}_0+\hat{\theta}_1\mu_X-Y_k)}}{n\sqrt{\det\left(2\pi(\hat{\theta}_1^T\hat{\theta}_1\sigma_X^2+\epsilon_T^2)\right)}} \\
&\quad + \frac{n+2\sum_{i,j=1,i<j}^n e^{-\frac{1}{2}(Y_i-Y_j)^T(2\epsilon_T^2\mathbf{I}_d)^{-1}(Y_i-Y_j)}}{n^2\sqrt{\det(4\pi\epsilon_T^2)}}
\end{aligned} \tag{3.14}$$

and

$$\begin{aligned}
& E_{OG}(\{(X_k, Y_k), k = 1, 2, \dots, n\}) \\
&= \frac{1}{\sqrt{\det(4\pi\hat{\theta}_1^T\hat{\theta}_1\sigma_X^2)}} - 2 \sum_{k=1}^N \frac{e^{-\frac{1}{2}(\hat{\theta}_0+\hat{\theta}_1\mu_X-Y_k)^T(\hat{\theta}_1^T\hat{\theta}_1\sigma_X^2+\epsilon_O^2)^{-1}(\hat{\theta}_0+\hat{\theta}_1\mu_X-Y_k)}}{N\sqrt{\det\left(2\pi(\hat{\theta}_1^T\hat{\theta}_1\sigma_X^2+\epsilon_O^2)\right)}} \\
&\quad + \frac{N+2\sum_{i,j=1,i<j}^N e^{-\frac{1}{2}(Y_i-Y_j)^T(2\epsilon_O^2\mathbf{I}_d)^{-1}(Y_i-Y_j)}}{N^2\sqrt{\det(4\pi\epsilon_O^2)}}
\end{aligned} \tag{3.15}$$

with $\epsilon_T^2 = \hat{\Sigma}_O/n^{2/d}$, $\epsilon_O^2 = \hat{\Sigma}_O/N^{2/d}$, here $\hat{\Sigma}_O$ is the covariance inferred from N data-points. By performing several simulations over the training set $\{(X_k, Y_k), k = 1, 2, \dots, n\}$ we have plotted the average value of the probability of $\Delta > 0$ in Fig. 3. The important regions for n are the following:⁴

- For $n \ll d$, as we increase n , the probability of $\Delta > 0$ increases sharply. We call this memorization to non-memorization transition.
- At $n \sim d$, the probability of $\Delta > 0$ saturates near unity and we enter at the regime where the Hellinger distance between the original and generated distribution H^2 decreases relatively faster. This shows the initiation of non-memorization is caused by the decay of generalization error.

4 Non-linear diffusion model

In this section we set up experiments on non-linear diffusion models. We use the PyTorch-based implementation of the algorithm in [3] as the diffusion model for the experiments in this section.⁵ The denoiser has the structure of U-Net [32] with additional residual connections consisting of positional encoding of the image and attention layers [33–35].

⁴For $N \sim n \gg d$: In this domain $P(\Delta > 0)$ decreases and eventually reaches the value 0.5. This is because the distinction between the train and the original dataset disappears in this limit.

⁵The computational might be further optimized with the energy-conserving descent method [31].

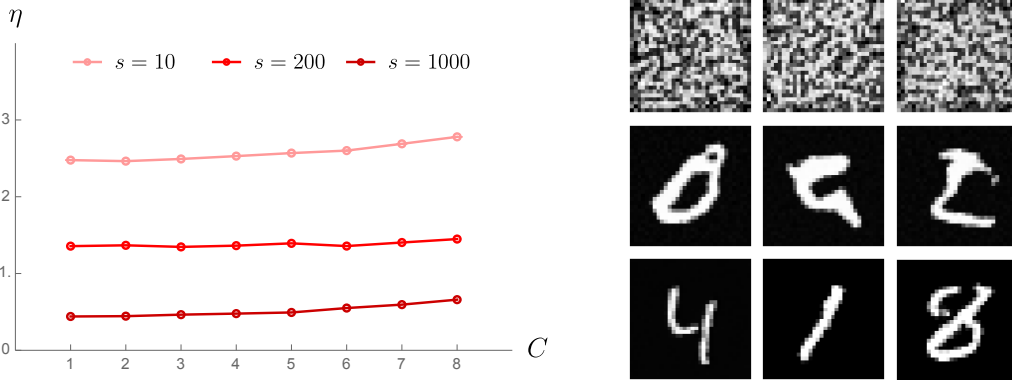


Figure 4: The plot is based on the neural network-based diffusion model with 12.9 million trainable parameters trained on equal weight Gaussian mixture model (GMM) with C components $i = 0, 1, 2, \dots, C - 1$ of dimension $d = 64$. The i -th component is an isotropic Gaussian of mean $\mu_i = \mu_0 + (i - (C - 1)/2)\sigma_0$, $\mu_0 = 0.5$ and standard deviation $\sigma_i = 0.1$. The number of samples in the original dataset is $N = 10^4$. Training is done for 10 epoch with batch size 128. The plot on the left shows a linear dependence of error $\eta = -\log(1 - E_{OG}(d/n \rightarrow 0)/E_{OG}(d/n \rightarrow \infty))$ on sample complexity C . In practice we have chosen $n = 50,4550$ and $d = 64$ at $s = 1000$ for example. The intercept and the slope of the linear graph depends on the hyper-parameters of the model, in particular we have plotted different curves for different diffusion steps s . The plot shows clearly that larger diffusion steps is better based on the experiments on Gaussian mixture model. On the right, we have generated images from the model with same hyper-parameter configurations on MNIST dataset. We see that the conclusion in GMM about production quality remains valid in MNIST dataset indicating an universal behavior.

Our definition in (3.12), (3.13) when supplemented with a similar definition for the generated distribution from a realistic diffusion model allows us to systemically study generalization properties of the model. For this purpose, we use the following simplified metric, which gives an advantage in terms of computational expense

$$E_{OG} = \sum_{i=1}^d \int dx (\rho_{O,i}(x) - \rho_{G,i}(x))^2, \quad (4.1)$$

$$\rho_{O,i}(x) \equiv \frac{1}{N} \sum_{k=1}^N \mathcal{N}(x|x_k^i, \epsilon_{O,i}^2), \quad \epsilon_{O,i}^2 = \frac{\hat{\Sigma}_{O,i}}{N^2}$$

Where we have defined element-wise probability density function. Similar definition applies to $\rho_{O,i}$, $\rho_{G,i}$ and E_{OG} . In addition we define production quality index $\eta =$

$-\log(1 - E_{OG}(d/n \rightarrow 0)/E_{OG}(d/n \rightarrow \infty))$. Smaller the value of η , the better the quality of the generated images.

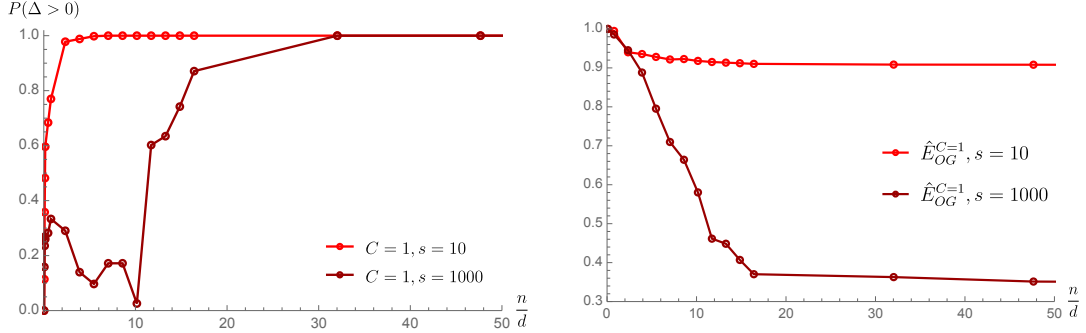


Figure 5: The model set up and dataset are the same as that in Fig. 4. \hat{E}_{OG} is the scaled value of E_{OG} by its value at $n = 10$. Just like the linear model discussed previously, we see that the memorization to non-memorization transition marked by the sharp increase of $P(\Delta > 0)$ (on left) takes place due to decay of generalization error \hat{E}_{OG} with addition of more training samples (on right). Plot on the left, further shows that the increasing diffusion steps does not necessarily help in reducing memorization. Plot on the right shows increasing diffusion steps does help the production quality of the model. It also shows that performance of the model flatten out as $n/d \rightarrow \infty$ and the asymptotic performance is dictated by the hyperparameters of the model.

From figure 4, it is clear that production quality of the model improves with higher diffusion steps s . This fact can be explained intuitively as follows. In the diffusion model we start from a clear image Y_0 and then obtain noisy images for steps $t = 1, 2, \dots, s$ from $Y_t = \sqrt{1 - \beta_t}Y_{t-1} + \sqrt{\lambda}\sqrt{\beta_t}Z, Z \sim \mathcal{N}(0, \mathbf{I}_d)$. Where $\beta_t = (t/s)\beta = 1 - e^{-\beta t/s} + \mathcal{O}(\beta^2), \beta \ll 1$ is the noise scheduler. If instead of using a non-linear neural network we use the linear denoiser to predict a Gaussian approximation of Y_{t-1} from Y_t we can use the argument below lemma 3.3 and find that $\text{KL}_{\text{var}}(t)/d \sim \lambda^2\beta_t^2/(1 - \beta_t)^2 \approx \lambda^2\beta^2(t/s)^2$. This shows that performance of the final denoising step is improved by a factor of s^2 compared to single step diffusion. In fact, performance of each step improves except the first one between Y_s, Y_{s-1} which remain the same. This suggests as we increase s overall production quality of the model will improve in agreement with the findings in figure 4. This argument also predicts that we need to have $\lambda\beta \ll 1$ for good quality generated images. In figure 4, in addition we have studied the performance of the diffusion model based on our metric on Gaussian mixture models and found an interesting relationship of the performance against sample complexity. See the figure for more details.

Following the results of the linear diffusion model, we hypothesize that a generic diffusion model features memorization to non-memorization transition due to decay in generalization error. Our hypothesis is confirmed in figure 5. In addition the plot of the left shows that increasing diffusion steps does not necessarily help mitigating memorization. This is consistent with the fact that an exact forward and reverse diffusion process would lead to perfect memorization of the training data [22]. On the other hand, plot on the right shows that higher diffusion step size leads to better production quality when unlimited training data is available. Putting these two facts together suggests there exists an optimal value of diffusion step given a finite training dataset size.

5 Acknowledgements

I.H. is grateful to Cengiz Pehlevan for mentioning the question, initial collaboration, and several insightful discussions throughout the project. I.H. would like to thank Alexander Atanasov, Hugo Cui, Sab Sainathan, Binxu Wang, and Jacob Zavaton-Veth for useful discussions. The numerical calculations presented in this paper are performed on the clusters of the Kempner Institute for the Study of Natural and Artificial Intelligence at Harvard University and Harvard John A. Paulson School Of Engineering And Applied Sciences. I. H. is supported by U.S. Department of Energy grant DE-SC0009999 and funds from the University of California.

References

- [1] J. Sohl-Dickstein, E.A. Weiss, N. Maheswaranathan and S. Ganguli, *Deep unsupervised learning using nonequilibrium thermodynamics*, 2015.
- [2] Y. Song and S. Ermon, *Generative modeling by estimating gradients of the data distribution*, *Advances in neural information processing systems* **32** (2019) .
- [3] J. Ho, A. Jain and P. Abbeel, *Denoising diffusion probabilistic models*, 2020.
- [4] A. Ramesh, P. Dhariwal, A. Nichol, C. Chu and M. Chen, *Hierarchical text-conditional image generation with clip latents*, 2022.
- [5] R. Rombach, A. Blattmann, D. Lorenz, P. Esser and B. Ommer, *High-resolution image synthesis with latent diffusion models*, 2022.
- [6] C. Saharia, W. Chan, S. Saxena, L. Li, J. Whang, E. Denton et al., *Photorealistic text-to-image diffusion models with deep language understanding*, 2022.
- [7] OpenAI, *Sora*, 2024, <https://openai.com/index/sora/>.
- [8] G. Somepalli, V. Singla, M. Goldblum, J. Geiping and T. Goldstein, *Diffusion art or digital forgery? investigating data replication in diffusion models*, 2022.

- [9] N. Carlini, J. Hayes, M. Nasr, M. Jagielski, V. Sehwag, F. Tramèr et al., *Extracting training data from diffusion models*, 2023.
- [10] Z. Kadkhodaie, F. Guth, E.P. Simoncelli and S. Mallat, *Generalization in diffusion models arises from geometry-adaptive harmonic representation*, *arXiv preprint arXiv:2310.02557* (2023) .
- [11] Z. Kadkhodaie and E.P. Simoncelli, *Solving linear inverse problems using the prior implicit in a denoiser*, in *NeurIPS 2020 Workshop on Deep Learning and Inverse Problems*, 2020, <https://openreview.net/forum?id=RLN7K4U3UST>.
- [12] J. Song, C. Meng and S. Ermon, *Denoising diffusion implicit models*, in *International Conference on Learning Representations*, 2021, <https://openreview.net/forum?id=St1giarCHLP>.
- [13] P. Dhariwal and A. Nichol, *Diffusion models beat gans on image synthesis*, 2021.
- [14] J. Ho and T. Salimans, *Classifier-free diffusion guidance*, 2022.
- [15] Y. Wu, M. Chen, Z. Li, M. Wang and Y. Wei, *Theoretical insights for diffusion guidance: A case study for gaussian mixture models*, 2024.
- [16] A. Bradley and P. Nakkiran, *Classifier-free guidance is a predictor-corrector*, 2024.
- [17] M. Chidambaram, K. Gatmiry, S. Chen, H. Lee and J. Lu, *What does guidance do? a fine-grained analysis in a simple setting*, 2024.
- [18] T. Karras, M. Aittala, T. Aila and S. Laine, *Elucidating the design space of diffusion-based generative models*, 2022.
- [19] T. Yoon, J.Y. Choi, S. Kwon and E.K. Ryu, *Diffusion probabilistic models generalize when they fail to memorize*, in *ICML 2023 Workshop on Structured Probabilistic Inference & Generative Modeling*, 2023, <https://openreview.net/forum?id=shciCbSk9h>.
- [20] M. Okawa, E.S. Lubana, R.P. Dick and H. Tanaka, *Compositional abilities emerge multiplicatively: Exploring diffusion models on a synthetic task*, 2024.
- [21] A. Sclocchi, A. Favero and M. Wyart, *A phase transition in diffusion models reveals the hierarchical nature of data*, 2024.
- [22] M. Kamb and S. Ganguli, *An analytic theory of creativity in convolutional diffusion models*, 2024.
- [23] A. Hyvärinen, *Estimation of non-normalized statistical models by score matching*, *Journal of Machine Learning Research* **6** (2005) 695.
- [24] B. Sriperumbudur, K. Fukumizu, A. Gretton, A. Hyvärinen and R. Kumar, *Density estimation in infinite dimensional exponential families*, 2017.
- [25] P. Vincent, *A connection between score matching and denoising autoencoders*, *Neural Computation* **23** (2011) 1661.
- [26] D. Gross and M. Mezard, *The simplest spin glass*, *Nuclear Physics B* **240** (1984) 431.

- [27] G. Biroli, T. Bonnaire, V. de Bortoli and M. Mézard, *Dynamical regimes of diffusion models*, 2024.
- [28] M. Rosenblatt, *Remarks on Some Nonparametric Estimates of a Density Function*, *The Annals of Mathematical Statistics* **27** (1956) 832 .
- [29] V.A. Epanechnikov, *Non-parametric estimation of a multivariate probability density*, *Theory of Probability & Its Applications* **14** (1969) 153 [<https://doi.org/10.1137/1114019>].
- [30] P.J. Bickel and M. Rosenblatt, *On Some Global Measures of the Deviations of Density Function Estimates*, *The Annals of Statistics* **1** (1973) 1071 .
- [31] G.B. De Luca and E. Silverstein, *Born-in-feld (bi) for ai: Energy-conserving descent (ecd) for optimization*, in *International Conference on Machine Learning*, pp. 4918–4936, PMLR, 2022.
- [32] O. Ronneberger, P. Fischer and T. Brox, *U-net: Convolutional networks for biomedical image segmentation*, 2015.
- [33] A. Dosovitskiy, L. Beyer, A. Kolesnikov, D. Weissenborn, X. Zhai, T. Unterthiner et al., *An image is worth 16x16 words: Transformers for image recognition at scale*, in *International Conference on Learning Representations*, 2021, <https://openreview.net/forum?id=YicbFdNTTy>.
- [34] Z. Tu, H. Talebi, H. Zhang, F. Yang, P. Milanfar, A. Bovik et al., *Marvit: Multi-axis vision transformer*, in *European conference on computer vision*, pp. 459–479, Springer, 2022.
- [35] W. Peebles and S. Xie, *Scalable diffusion models with transformers*, in *Proceedings of the IEEE/CVF International Conference on Computer Vision*, pp. 4195–4205, 2023.
- [36] M.S. Albergo, N.M. Boffi and E. Vanden-Eijnden, *Stochastic interpolants: A unifying framework for flows and diffusions*, 2023.
- [37] Y. Song, J. Sohl-Dickstein, D.P. Kingma, A. Kumar, S. Ermon and B. Poole, *Score-based generative modeling through stochastic differential equations*, 2021.
- [38] A. Atanasov, J.A. Zavattone-Veth and C. Pehlevan, *Scaling and renormalization in high-dimensional regression*, 2024.
- [39] A. Jacot, F. Gabriel and C. Hongler, *Neural tangent kernel: Convergence and generalization in neural networks*, 2020.
- [40] A. Jacot, F. Gabriel and C. Hongler, *Neural tangent kernel: Convergence and generalization in neural networks*, in *Advances in Neural Information Processing Systems*, S. Bengio, H. Wallach, H. Larochelle, K. Grauman, N. Cesa-Bianchi and R. Garnett, eds., vol. 31, Curran Associates, Inc., 2018, https://proceedings.neurips.cc/paper_files/paper/2018/file/5a4be1fa34e62bb8a6ec6b91d2462f5a-Paper.pdf.
- [41] J. Lee, L. Xiao, S. Schoenholz, Y. Bahri, R. Novak, J. Sohl-Dickstein et al., *Wide neural networks of any depth evolve as linear models under gradient descent*, in

- Advances in Neural Information Processing Systems*, H. Wallach, H. Larochelle, A. Beygelzimer, F. d'Alché-Buc, E. Fox and R. Garnett, eds., vol. 32, Curran Associates, Inc., 2019, https://proceedings.neurips.cc/paper_files/paper/2019/file/0d1a9651497a38d8b1c3871c84528bd4-Paper.pdf.
- [42] B. Bordelon, A. Canatar and C. Pehlevan, *Spectrum dependent learning curves in kernel regression and wide neural networks*, 2021.
- [43] A. Canatar, B. Bordelon and C. Pehlevan, *Spectral bias and task-model alignment explain generalization in kernel regression and infinitely wide neural networks*, *Nature Communications* **12** (2021) .
- [44] D.A. Roberts, S. Yaida and B. Hanin, *The Principles of Deep Learning Theory: An Effective Theory Approach to Understanding Neural Networks*, Cambridge University Press (May, 2022), [10.1017/9781009023405](https://doi.org/10.1017/9781009023405).
- [45] A. Atanasov, B. Bordelon, S. Sainathan and C. Pehlevan, *The onset of variance-limited behavior for networks in the lazy and rich regimes*, in *The Eleventh International Conference on Learning Representations*, 2023, <https://openreview.net/forum?id=JLINxPOVTh7>.
- [46] M. Demirtas, J. Halverson, A. Maiti, M.D. Schwartz and K. Stoner, *Neural network field theories: Non-gaussianity, actions, and locality*, 2023.
- [47] S. Mei, A. Montanari and P.-M. Nguyen, *A mean field view of the landscape of two-layer neural networks*, *Proceedings of the National Academy of Sciences* **115** (2018) .
- [48] G. Yang and E.J. Hu, *Tensor programs iv: Feature learning in infinite-width neural networks*, in *Proceedings of the 38th International Conference on Machine Learning*, M. Meila and T. Zhang, eds., vol. 139 of *Proceedings of Machine Learning Research*, pp. 11727–11737, PMLR, 18–24 Jul, 2021, <https://proceedings.mlr.press/v139/yang21c.html>.
- [49] B. Bordelon and C. Pehlevan, *Self-consistent dynamical field theory of kernel evolution in wide neural networks*, *Advances in Neural Information Processing Systems* **35** (2022) 32240.
- [50] B. Bordelon and C. Pehlevan, *Dynamics of finite width kernel and prediction fluctuations in mean field neural networks*, *Advances in Neural Information Processing Systems* **36** (2024) .

A Connection between ODE and SDE based generative models

In this Appendix we review the connection between stochastic interpolant [36] and stochastic differential equation [37] based generative models. Given two probability

density functions ρ_0, ρ_1 , one can construct a stochastic interpolant between ρ_0 and ρ_1 as follows

$$x(t) = X(t, x_0, x_1) + \lambda_0(t)z, \quad t \in [0, 1] \quad (\text{A.1})$$

where the function X, λ_0 satisfies

$$\begin{aligned} X(0, x_0, x_1) &= x_0, \quad X(1, x_0, x_1) = x_1, \quad \|\partial_t X(t, x_0, x_1)\| \leq C\|x_0 - x_1\| \\ \lambda_0(0) &= 0, \quad \lambda_0(1) = 0, \quad \lambda_0(t) \geq 0 \end{aligned} \quad (\text{A.2})$$

for some positive constant C . Here x_0, x_1, z are drawn independently from a probability measure ρ_0, ρ_1 and standard normal distribution $\mathcal{N}(0, \mathbf{I})$. The probability distribution $\rho(t, x)$ of the process $x(t)$ satisfies the transport equation⁶

$$\partial_t \rho + \nabla \cdot (b\rho) = 0, \quad \rho(0, x) = \rho_0(x), \quad \rho(1, x) = \rho_1(x), \quad (\text{A.3})$$

where we defined the velocity⁷

$$b(t, x) = \mathbb{E}[\dot{x}(t)|x(t) = x] = \mathbb{E}[\partial_t X(t, x_0, x_1) + \dot{\lambda}_0(t)z|x(t) = x]. \quad (\text{A.4})$$

One can estimate the velocity field by minimizing

$$L_b[\hat{b}] = \int_0^1 \mathbb{E} \left(\frac{1}{2} \|\hat{b}(t, x(t))\|^2 - \left(\partial_t X(t, x_0, x_1) + \dot{\lambda}_0(t)z \right) \cdot \hat{b}(t, x(t)) \right) dt \quad (\text{A.5})$$

It's useful to introduce the score function $s(t, x)$ for the probability distribution for making the connection to the stochastic differential equation

$$s(t, x) = \nabla \log \rho(t, x) = -\lambda_0^{-1}(t)\mathbb{E}(z|x(t) = x) \quad (\text{A.6})$$

It can be estimated by minimizing

$$L_s[\hat{s}] = \int_0^1 \mathbb{E} \left(\frac{1}{2} \|\hat{s}(t, x(t))\|^2 + \lambda_0^{-1}(t)z \cdot \hat{s}(t, x(t)) \right) dt \quad (\text{A.7})$$

The score function also can be obtained by minimizing the following alternative objective function known as the Fisher divergence

$$\begin{aligned} L_F[\hat{s}] &= \frac{1}{2} \int_0^1 \mathbb{E} \left(\|\hat{s}(t, x(t)) - \nabla \log \rho(t, x)\|^2 \right) dt \\ &= \int_0^1 \mathbb{E} \left(\frac{1}{2} \|\hat{s}(t, x(t))\|^2 + \nabla \cdot \hat{s}(t, x(t)) + \frac{1}{2} \|\nabla \log \rho(t, x)\|^2 \right) dt \end{aligned} \quad (\text{A.8})$$

To obtain the second line we have ignored the boundary term. Note that for the purpose of minimization the last term is a constant and hence it plays no role hence

⁶Here we are using the notation $\nabla = \nabla_x$.

⁷The expectation is taken independently over $x_0 \sim \rho_0, x_1 \sim \rho_1$ and $z \sim \mathcal{N}(0, \mathbf{I})$. Here $\mathcal{N}(0, \mathbf{I})$ is normalized Gaussian distribution of appropriate dimension with vanishing mean and variance.

Fisher divergence can be minimized from a set of samples drawn from ρ easily even if the explicit form of ρ is not known [23]. However, the estimation of $\nabla \cdot \hat{s}(t, x(t))$ is computationally expensive and in practice one uses denoising score matching for estimating the score function [25].

It is easy to put eq. (A.3) into Fokker-Planck-Kolmogorov form

$$\begin{aligned}\partial_t \rho + \nabla \cdot (b_F \rho) &= +\lambda(t) \Delta \rho, & b_F(t, x) &= b(t, x) + \lambda(t) s(t, x) \\ \partial_t \rho + \nabla \cdot (b_B \rho) &= -\lambda(t) \Delta \rho, & b_B(t, x) &= b(t, x) - \lambda(t) s(t, x)\end{aligned}\quad (\text{A.9})$$

For an arbitrary function $\lambda(t) \geq 0$. From this, we can read off the Itô SDE as follows⁸

$$\begin{aligned}dX_t^F &= b_F(t, X_t^F) dt + \sqrt{2\lambda(t)} dW_t \\ dX_t^B &= b_B(t, X_t^B) dt - \sqrt{2\lambda(t)} dW_{1-t}\end{aligned}\quad (\text{A.10})$$

The first equation is solved forward in time from the initial data $X_{t=0}^F \sim \rho_0$ and the second one is solved backward in time from the final data $X_{t=1}^B \sim \rho_1$. One can recover the probability distribution ρ from the SDE using Feynman–Kac formulae⁹

$$\begin{aligned}\rho(t, x) &= \mathbb{E} \left(e^{\int_t^0 \nabla \cdot b_F(t, Y_t^B) dt} \rho_0(Y_{t=0}^B) | Y_t^B = x \right) \\ &= \mathbb{E} \left(e^{\int_t^1 \nabla \cdot b_B(t, Y_t^F) dt} \rho_1(Y_{t=1}^F) | Y_t^F = x \right)\end{aligned}\quad (\text{A.12})$$

B Principle of deterministic equivalence

In this appendix we review the theory of large random matrices leading to the principle of deterministic equivalence. A $d \times d$ Hermitian random matrix A with measure $d\mu_A$ is called an invariant random matrix if the measure satisfies

$$d\mu_A(A) = d\mu_A(U^\dagger A U) \quad (\text{B.1})$$

for any unitary matrix U . In the limit of $d \rightarrow \infty$, the theory is conveniently described in terms of the single eigenvalue density ρ_A (normalized to unity) that can be obtained from the resolvent or the Stieltjes transform

$$G_A(z) = \left\langle \frac{1}{d} \text{Tr} \left(\frac{1}{z - A} \right) \right\rangle = \int \frac{\rho_A(\lambda) d\lambda}{z - \lambda} \implies \rho_A(\lambda) = -\frac{1}{\pi} \lim_{\epsilon \rightarrow 0^+} \Im(G_A(\lambda + i\epsilon)) \quad (\text{B.2})$$

⁸Here W_t represents a standard Wiener process, i.e., $W_t - tW_1 = N_t$ is a zero-mean Gaussian stochastic process that satisfies $\mathbb{E}[N_t N_t^\top] = t(1-t)\mathbf{I}$.

⁹A class of exactly solvable models are given by (Ornstein-Uhlenbeck dynamics discussed in the main text is a special case of this equation)

$$dX_t^F = X_t^F \frac{d}{dt} (\log \eta(t)) dt + \sqrt{\eta(t)^2 \frac{d}{dt} \left(\frac{\sigma(t)^2}{\eta(t)^2} \right)} dW_t, \quad X_t^F \sim \mathcal{N}(\eta(t) X_0^F, \sigma(t)^2) \quad (\text{A.11})$$

Where η, σ are two positive functions satisfying $\eta(0) = 1, \sigma(0) = 0$.

The moment generating function is given by

$$M_A(z) = \frac{1}{z} G_A\left(\frac{1}{z}\right) - 1 = \left\langle \frac{1}{d} \text{Tr} \sum_{i=1}^{\infty} A^i z^i \right\rangle \quad (\text{B.3})$$

R, S transformation of the eigenvalue density are defined by

$$\begin{aligned} R_A(z) &= G_A^{inv}(z) - \frac{1}{z}, & G_A^{inv}(G_A(z)) &= z \\ S_A(z) &= \frac{z+1}{z} M_A^{inv}(z), & M_A^{inv}(M_A(z)) &= z \end{aligned} \quad (\text{B.4})$$

R, S transformations are useful when we study the matrix model to the leading order in large d limit as we explain next. Two invariant random matrices A, B are called free to the leading order in large d limit if they are independent. Free sum and free product of A, B are defined as follows

$$\begin{aligned} A \boxplus B &= U^\dagger A U + V^\dagger B V \\ A \star B &= \sqrt{A} B \sqrt{A} \end{aligned} \quad (\text{B.5})$$

Here U, V are sampled independently from uniform measure on the unitary group, i.e., Haar random unitary. It can be shown that for two invariant, independent random matrices A, B the moment generating function of $A \boxplus B$ and $A+B$ coincides, similarly moment generating function of $A \star B$ and AB coincides (to the leading order in large d , i.e., when they are free). Furthermore following identity holds to the leading order in large d limit for two free matrices A, B

$$R_{A \boxplus B}(z) = R_A(z) + R_B(z), \quad S_{A \star B}(z) = S_A(z) S_B(z) \quad (\text{B.6})$$

Now we turn to application of these ideas. Consider $d \times d$ matrix $\hat{\Sigma} = x^T x / n$ where each row of x (there are n rows) is drawn from $\mathcal{N}(0, \Sigma)$. Then it can be written as a free product of Σ and a white Wishart matrix W (corresponds to $x^T x / n$ where each row of x is drawn from $\mathcal{N}(0, \mathbf{I}_d)$): $\hat{\Sigma} = \Sigma \star W$. From the definition of S transformation it follows that

$$M_{\hat{\Sigma}}(z) = \frac{1}{\frac{S_{\hat{\Sigma}}(M_{\hat{\Sigma}}(z))}{z} - 1} = \frac{1}{\frac{S_{\Sigma}(M_{\hat{\Sigma}}(z)) S_W(M_{\hat{\Sigma}}(z))}{z} - 1} = M_{\Sigma}\left(\frac{z}{S_W(M_{\hat{\Sigma}}(z))}\right) \quad (\text{B.7})$$

To obtain the final equality we used self-consistency of the equation itself. To recast this equation in a compact way we define $df_A^1(z) = -M_A(-1/z) = \langle \text{Tr} \hat{\Sigma} (\hat{\Sigma} + \hat{R})^{-1} \rangle / d$. In terms of this new quantity we have

$$df_{\hat{\Sigma}}^1(\hat{R}) = df_{\Sigma}^1(R), \quad \hat{R} = R(1 - \alpha df_{\Sigma}^1(R)) \quad (\text{B.8})$$

To obtain this equation we used knowledge of S transformation of white Wishart matrices $S_W(z) = 1/(1 + \alpha z)$, $\alpha = d/n$. This equation is valid only leading order in large d, n limit with fixed α . It is known as the principle of deterministic equivalence. See [38] and references therein for a recent discussion of it.

C Generalization error from deterministic equivalence

In this appendix, we provide proof of the main theorem in the paper (3.6), (3.7). Consider the scenario when the underlying sampling distribution is an isotropic Gaussian $\rho = \mathcal{N}(\mu, \sigma^2 I_d)$. The linear diffusion model $Y = \theta_0 + \theta_1 X$ is trained to solve the following linear regression problem

$$\begin{aligned} Y_k &= e^T X_k + Z_k, \quad X_k \sim \mathcal{N}(\mu_X, \Sigma = \sigma_X^2 I_d), \quad Z_k \sim \mathcal{N}(0, \Delta_T I_d), \quad k = 1, \dots, n \\ \mu_X &= e^{-T} \mu, \quad \sigma_X^2 = e^{-2T} \sigma^2 + \Delta_T, \quad \Delta_T = \lambda(1 - e^{-2T}) \end{aligned} \quad (\text{C.1})$$

The optimal value of the weights $\hat{\theta}_0, \hat{\theta}_1$ that minimizes the standard square loss are given by

$$\hat{\theta}_1^T = (x^T x + n\hat{R})^{-1} x^T y, \quad \hat{\theta}_0 = \hat{Y} - \hat{\theta}_1 \hat{X} \quad \hat{X} = \frac{1}{n} \sum_{k=1}^n X_k, \quad \hat{Y} = \frac{1}{n} \sum_{k=1}^n Y_k \quad (\text{C.2})$$

Here x, y are $n \times d$ dimensional matrices whose k -th row is $(X_k - \hat{X})^T, (Y_k - \hat{Y})^T$ respectively (e.g. $x_{iA} = (X_i - \hat{X})_A$ etc.) and \hat{R} is a scalar ridge parameter. Once trained the diffusion model generates data from $\rho_G = \mathcal{N}(\hat{\mu}_G, \hat{\Sigma}_G)$, $\hat{\mu}_G = \hat{\theta}_0 + \hat{\theta}_1 \mu_X$, $\hat{\Sigma}_G = \sigma_X^2 \hat{\theta}_1^T \hat{\theta}_1$.

KL divergence between two PDF $\rho_1 = \mathcal{N}(\mu_1, \Sigma_1), \rho_2 = \mathcal{N}(\mu_2, \Sigma_2)$ is given by

$$\begin{aligned} \text{KL}(\rho_1 | \rho_2) &= \int \rho_1(x) \log \frac{\rho_1(x)}{\rho_2(x)} dx \\ &= \frac{\text{Tr}(\Sigma_2^{-1} \Sigma_1) - \text{Tr}(I)}{2} - \frac{1}{2} \log |\Sigma_2^{-1} \Sigma_1| + \frac{1}{2} (\mu_1 - \mu_2)^T \Sigma_2^{-1} (\mu_1 - \mu_2) \end{aligned} \quad (\text{C.3})$$

We choose $\mu_2 = \mu, \Sigma_2 = \sigma^2 I_d$ to correspond to the underlying distribution and $\mu_1 = \hat{\mu}_G, \Sigma_1 = \hat{\Sigma}_G$ corresponds to the generated distribution. This simplifies the formula above to

$$\begin{aligned} \text{KL}(\rho_G | \rho) &= \frac{1}{2} (\text{Tr} \left(\frac{\hat{\Sigma}_G}{\sigma^2} \right) - \text{Tr}(I)) - \frac{1}{2} \text{Tr} \log \left(\frac{\hat{\Sigma}_G}{\sigma^2} \right) + \frac{1}{2\sigma^2} (\mu - \hat{\mu}_G)^T (\mu - \hat{\mu}_G) \\ &\geq \frac{1}{2} (\text{Tr} \left(\frac{\hat{\Sigma}_G}{\sigma^2} \right) - \text{Tr}(I)) - \frac{1}{2} \text{Tr} \log \left(\frac{\hat{\Sigma}_G}{\sigma^2} \right) \end{aligned} \quad (\text{C.4})$$

To go to the second line we have ignored the positive semi-definite term related to difference in mean between generated and underlying distribution. We proceed to calculate the variance term in KL divergence above. It follows that

$$\begin{aligned} \hat{\theta}_1^T &= (x^T x + n\hat{R})^{-1} x^T y \\ &= (x^T x + n\hat{R})^{-1} x^T (x\bar{\theta}_1^T + z) \\ &= e^T (1 - \hat{R}(\hat{\Sigma} + \hat{R})^{-1}) + (\hat{\Sigma} + \hat{R})^{-1} \frac{x^T z}{n} \end{aligned} \quad (\text{C.5})$$

We have defined $\bar{\theta}_1 = e^T I_d$, $\hat{\Sigma} = x^T x/n$ for later convenience. Next we calculate

$$\begin{aligned}\hat{\theta}_1^T \hat{\theta}_1 &= \bar{\theta}_1^T \bar{\theta}_1 + \hat{\Sigma}_{\theta_1} \\ \hat{\Sigma}_{\theta_1} &= (\hat{\Sigma} + \hat{R})^{-1} \frac{x^T z}{n} \frac{z^T x}{n} (\hat{\Sigma} + \hat{R})^{-1} + e^{2T} \hat{R}^2 (\hat{\Sigma} + \hat{R})^{-2} - 2e^{2T} \hat{R} (\hat{\Sigma} + \hat{R})^{-1} \\ &\quad + e^T \left(\frac{z^T x}{n} (\hat{\Sigma} + \hat{R})^{-1} + (\hat{\Sigma} + \hat{R})^{-1} \frac{x^T z}{n} \right) - e^T \hat{R} (\hat{\Sigma} + \hat{R})^{-1} \left(\frac{z^T x}{n} + \frac{x^T z}{n} \right) (\hat{\Sigma} + \hat{R})^{-1}\end{aligned}\tag{C.6}$$

Plugging this back in the expression of $\hat{\Sigma}_G$ we get

$$\begin{aligned}\frac{\hat{\Sigma}_G}{\sigma^2} &= (1 + \sigma^{-2} e^{2T} \Delta_T) (I + e^{-2T} \hat{\Sigma}_{\theta_1}) = I + \hat{\sigma}_G \\ \hat{\sigma}_G &= (e^{-2T} + \sigma^{-2} \Delta_T) \hat{\Sigma}_{\theta_1} + e^{2T} \sigma^{-2} \Delta_T I\end{aligned}\tag{C.7}$$

Appearance of logarithm in the KL divergence makes it difficult to calculate its statistical expectation value. In next sub-section we develop a controlled expansion for this purpose.

Analytic tractability and various approximations

From (C.7) we see that the generated distribution remains close to the original underlying distribution if both Δ_T and $\hat{\sigma}_G$ remain small. To this end, we focus on the following limit:

$\lambda = \hat{\lambda} \sigma^2 e^{-2T}$, $\hat{R} = \lambda \hat{r}$. In this regime $\hat{\sigma}_G \sim \hat{\lambda}$. Further taking $\hat{\lambda} \ll 1$ makes $\hat{\sigma}_G$ small and we can approximate

$$\log \left(\frac{\hat{\Sigma}_G}{\sigma^2} \right) = \log(I + \hat{\sigma}_G) = \hat{\sigma}_G - \frac{1}{2} \hat{\sigma}_G^2 + \mathcal{O}(\hat{\sigma}_G^3)\tag{C.8}$$

Plugging this back into the expression of KL divergence (C.4) we get $\text{KL}(\rho||\rho_G) = \text{KL}_{\text{mean}} + \text{KL}_{\text{var}}$, where

$$\text{KL}_{\text{mean}}(\rho_G|\rho) = \frac{1}{2\sigma^2} (\mu - \hat{\mu}_G)^T (\mu - \hat{\mu}_G), \quad \text{KL}_{\text{var}}(\rho_G|\rho) = \frac{1}{4} \text{Tr} \left(\left(\frac{\hat{\Sigma}_G}{\sigma^2} - I \right)^2 \right)\tag{C.9}$$

We focus on the variance term. Plugging back expressions from previous analysis

$$\begin{aligned}\text{KL}(\rho_G|\rho)_{\text{var}} &= \frac{1}{4} \text{Tr} \left(\frac{\hat{\Sigma}_G}{\sigma^2} - I \right)^2 = \frac{1}{4} \text{Tr} (\hat{\sigma}_G^2) \\ &= \frac{1}{4} \text{Tr} \left((e^{-2T} + \sigma^{-2} \Delta_T) \hat{\Sigma}_{\theta_1} + \sigma^{-2} e^{2T} \Delta_T \right)^2 \\ &= \frac{1}{4} (e^{-2T} + \sigma^{-2} \Delta_T)^2 \text{Tr} \hat{\Sigma}_{\theta_1}^2 \\ &\quad + \frac{1}{2} (e^{-2T} + \sigma^{-2} \Delta_T) \sigma^{-2} e^{2T} \Delta_T \text{Tr} \hat{\Sigma}_{\theta_1} + \frac{d}{4} (\sigma^{-2} e^{2T} \Delta_T)^2\end{aligned}\tag{C.10}$$

We are interested in statistical average of the expression above. We consider the following higher dimensional statistics limit: $n \rightarrow \infty, d \rightarrow \infty$ keeping $\alpha = d/n$ fixed. In this limit, we can take advantage of principle of deterministic equivalence discussed in previous appendix:

$$df_{\hat{\Sigma}}^1(\hat{R}) = df_{\Sigma}^1(R), \quad df_{\hat{\Sigma}}^n(\hat{R}) = \frac{1}{d} \langle \text{Tr} \hat{\Sigma}^n (\hat{\Sigma} + \hat{R})^{-n} \rangle, \quad \hat{R} = R(1 - \alpha df_{\Sigma}^1(R)) \quad (\text{C.11})$$

Since x, z are statistically independent and z has zero mean, we get

$$\text{Tr} \langle \hat{\Sigma}_{\theta_1} \rangle = \text{Tr} \langle (\hat{\Sigma} + \hat{R})^{-1} \frac{x^T z z^T x}{n} (\hat{\Sigma} + \hat{R})^{-1} + e^{2T} \hat{R}^2 (\hat{\Sigma} + \hat{R})^{-2} - 2e^{2T} \hat{R} (\hat{\Sigma} + \hat{R})^{-1} \rangle \quad (\text{C.12})$$

The first term is simplified after performing statistical average over z

$$(x^T z z^T x)_{AB} = x_{Ai}^T z_{iC} z_{jC} x_{jB} \rightarrow nd \Delta_T \hat{\Sigma}_{AB} \quad (\text{C.13})$$

The factor of d came from sum over C (we are using the convention of repeated index implies sum). The first term becomes $\alpha \Delta_T$ times

$$\text{Tr} \langle (\hat{\Sigma} + \hat{R})^{-1} \hat{\Sigma} (\hat{\Sigma} + \hat{R})^{-1} \rangle = \text{Tr} \langle \hat{\Sigma} (\hat{\Sigma} + \hat{R})^{-2} \rangle = -\partial_{\hat{R}} \langle \text{Tr} \hat{\Sigma} (\hat{\Sigma} + \hat{R})^{-1} \rangle = -d \partial_{\hat{R}} \langle df_{\Sigma}^1(R) \rangle \quad (\text{C.14})$$

For the case we are considering,

$$df_{\Sigma=\sigma_X^2 I_d}^1(R) = df_{\Sigma=I_d}^1(\sigma_X^{-2} R) = \frac{1}{1 + \sigma_X^{-2} R} \quad (\text{C.15})$$

Putting these expressions together the first term becomes

$$\alpha d \Delta_T \frac{\sigma_X^{-2}}{(1 + \sigma_X^{-2} R)^2} \partial_{\hat{R}} R = \alpha d \Delta_T \sigma_X^{-2} \frac{(df_{\Sigma}^1(R))^2}{1 - \alpha df_{\Sigma}^2(R)} \quad (\text{C.16})$$

To obtain the second line we have used the following identity

$$df_{\Sigma}^{n+1}(R) = \left(1 + \frac{R}{n} \partial_R \right) df_{\Sigma}^n(R), \quad \partial_{\hat{R}} R = \frac{1}{1 - \alpha df_{\Sigma}^2(R)} \quad (\text{C.17})$$

The third term is $-2e^{2T}$ times

$$\text{Tr} \langle \hat{R} (\hat{\Sigma} + \hat{R})^{-1} \rangle = d(1 - df_{\Sigma}^1(R)) \quad (\text{C.18})$$

The second term is e^{2T} times

$$\begin{aligned} \text{Tr} \langle (\hat{R} (\hat{\Sigma} + \hat{R})^{-1})^2 \rangle &= \text{Tr} \langle 1 - 2\hat{\Sigma} (\hat{\Sigma} + \hat{R})^{-1} + \hat{\Sigma}^2 (\hat{\Sigma} + \hat{R})^{-2} \rangle \\ &= d - 2d df_{\Sigma}^1(R) + d df_{\Sigma}^2(\hat{R}) \\ &= d - 2d df_{\Sigma}^1(R) + d \left(1 + \frac{\hat{R}}{1 - \alpha df_{\Sigma}^2(R)} \partial_R df_{\Sigma}^1(R) \right) \end{aligned} \quad (\text{C.19})$$

Combining all these we get

$$\begin{aligned} \text{Tr} \langle \hat{\Sigma}_{\theta_1} \rangle &= \alpha d \Delta_T \sigma_X^{-2} \frac{(df_{\Sigma}^1(R))^2}{1 - \alpha df_{\Sigma}^2(R)} - 2e^{2T} d(1 - df_{\Sigma}^1(R)) \\ &+ e^{2T} d \left(2 - 2 df_{\Sigma}^1(R) + \frac{\hat{R}}{1 - \alpha df_{\Sigma}^2(R)} \partial_R df_{\Sigma}^1(R) \right) \end{aligned} \quad (\text{C.20})$$

Now we turn to evaluate $\text{Tr} \langle \hat{\Sigma}_{\theta_1}^2 \rangle$. We want to keep track of terms that are order d and ignore sub-leading terms. This restricts possible contractions of z, z^T . We get a factor of d only from contractions that happen next to each other. Keeping only those terms

$$\begin{aligned} \text{Tr} \langle \hat{\Sigma}_{\theta_1}^2 \rangle &\approx \langle \alpha^2 \Delta_T^2 \text{Tr} (\hat{\Sigma}^2 (\hat{\Sigma} + \hat{R})^{-4}) + e^{4T} \hat{R}^4 \text{Tr} (\hat{\Sigma} + \hat{R})^{-4} + 4e^{4T} \hat{R}^2 \text{Tr} (\hat{\Sigma} + \hat{R})^{-2} \\ &+ 2\alpha \Delta_T e^{2T} \hat{R}^2 \text{Tr} (\hat{\Sigma} (\hat{\Sigma} + \hat{R})^{-4}) - 4\alpha \Delta_T e^{2T} \hat{R} \text{Tr} \hat{\Sigma} (\hat{\Sigma} + \hat{R})^{-3} - 4e^{4T} \hat{R}^3 \text{Tr} (\hat{\Sigma} + \hat{R})^{-3} \\ &+ 2\alpha \Delta_T e^{2T} \text{Tr} (\hat{\Sigma} (\hat{\Sigma} + \hat{R})^{-2}) \rangle \end{aligned} \quad (\text{C.21})$$

All these expectation values can be calculated from a generic term of the form for integer $a > 0, b \geq 0$

$$\begin{aligned} C_{a,b} &= \langle \text{Tr} (\hat{\Sigma}^a (\hat{\Sigma} + \hat{R})^{-(a+b)}) \rangle = \frac{(-1)^b}{a(a+1) \dots (a+b-1)} \partial_{\hat{R}}^b \langle \text{Tr} (\hat{\Sigma}^a (\hat{\Sigma} + \hat{R})^{-a}) \rangle \\ &= d \frac{\Gamma(a)}{\Gamma(a+b)} (-\partial_{\hat{R}})^b df_{\Sigma}^a(\hat{R}) \end{aligned} \quad (\text{C.22})$$

Another identity that is useful is the following

$$\begin{aligned} B_a &= \langle \text{Tr} \hat{R}^a (\hat{\Sigma} + \hat{R})^{-a} \rangle \\ &= \langle \text{Tr} (\hat{R}^{a-1} (\hat{\Sigma} + \hat{R})^{-(a-1)} - \hat{R}^{a-1} \hat{\Sigma} (\hat{\Sigma} + \hat{R})^{-a}) \rangle \\ &= \langle \text{Tr} (1 - \sum_{i=1}^a \hat{R}^{a-i} \hat{\Sigma} (\hat{\Sigma} + \hat{R})^{-(a-i+1)}) \rangle \\ &= d - \sum_{i=1}^a \hat{R}^{a-i} C_{1,a-i} \end{aligned} \quad (\text{C.23})$$

Now we turn to calculate expression for the symbols defined above. To get an explicit formula for $C_{a,b}$ first we replace the derivative with respect to \hat{R} by a derivative with respect to R with the chain rule given in the second equation on (C.17). Next we use the recursion relation in the first equation on (C.17) to express everything in terms of $df_{\Sigma}^1(\hat{R}) \simeq df_{\Sigma}^1(R)$. Finally to perform the derivatives we use the self-consistency equation of the ridge parameter given in the last equation on (C.11). Finally we use (C.15). Once $C_{a,b}$ s are computed we use the recursion relation to compute B_a s. The

expression for these quantities for $\alpha > 1$ are complicated. They are given as follows

$$B_1 = \begin{cases} \frac{dR}{R + \sigma_X^2} & \text{When } R(R + 2\sigma_X^2) \geq (\alpha - 1)\sigma_X^4 \\ d - \frac{d\left(\frac{R}{\sigma_X^2} + 1\right)}{\alpha} & \text{Otherwise} \end{cases} \quad (\text{C.24})$$

$$B_2 = \begin{cases} \frac{dR^2}{R^2 + 2R\sigma_X^2 - \alpha\sigma_X^4 + \sigma_X^4} & \text{When } R(R + 2\sigma_X^2) \geq (\alpha - 1)\sigma_X^4 \\ d\left(-\frac{1}{\alpha} - \frac{R^2}{R^2 + 2R\sigma_X^2 - \alpha\sigma_X^4 + \sigma_X^4} + 1\right) & \text{Otherwise} \end{cases} \quad (\text{C.25})$$

$$B_3 = \begin{cases} \frac{1}{(R^2 + 2R\sigma_X^2 - ((\alpha - 1)\sigma_X^4))^3} (dR^3 (3R^2\sigma_X^2 + R^3 + 3R\sigma_X^4 - ((\alpha^2 - 1)\sigma_X^6))) & \text{When } R(R + 2\sigma_X^2) \geq (\alpha - 1)\sigma_X^4 \\ \frac{1}{\alpha(-R^2 - 2R\sigma_X^2 + (\alpha - 1)\sigma_X^4)^3} (d(R - (\alpha - 1)\sigma_X^2)^3 (3R^2\sigma_X^2 + R^3 + 3R\sigma_X^4 - ((\alpha - 1)\sigma_X^6))) & \text{Otherwise} \end{cases} \quad (\text{C.26})$$

$$B_4 = \begin{cases} \frac{1}{(R^2 + 2R\sigma_X^2 - ((\alpha - 1)\sigma_X^4))^5} (dR^4 (4(-\alpha^2 + \alpha + 5)R^3\sigma_X^6 + (\alpha((\alpha - 12)\alpha + 6) + 15)R^2\sigma_X^8 + (\alpha + 15)R^4\sigma_X^4 + 6R^5\sigma_X^2 + R^6 + 2(\alpha((\alpha - 6)\alpha + 2) + 3)R\sigma_X^{10} + (\alpha - 1)^2(\alpha(\alpha + 3) + 1)\sigma_X^{12})) & \text{When } R(R + 2\sigma_X^2) \geq (\alpha - 1)\sigma_X^4 \\ \frac{1}{\alpha(-R^2 - 2R\sigma_X^2 + (\alpha - 1)\sigma_X^4)^5} (d(R - (\alpha - 1)\sigma_X^2)^4 (-5(\alpha - 3)R^2\sigma_X^8 + (\alpha + 15)R^4\sigma_X^4 + 20R^3\sigma_X^6 + 6R^5\sigma_X^2 + R^6 - 6(\alpha - 1)R\sigma_X^{10} + (\alpha - 1)^2\sigma_X^{12})) & \text{Otherwise} \end{cases} \quad (\text{C.27})$$

$$C_{1,1} = \frac{2d\sigma_X^2 (R + \sigma_X^2)^2}{| -((\alpha - 1)\sigma_X^4) + 2R\sigma_X^2 + R^2 | (| -((\alpha - 1)\sigma_X^4) + 2R\sigma_X^2 + R^2 | + R^2 + 2R\sigma_X^2 + (\alpha + 1)\sigma_X^4)} \quad (\text{C.28})$$

$$C_{1,2} = \frac{d\sigma_X^2 (R + \sigma_X^2)^3}{| -\alpha\sigma_X^4 + \sigma_X^4 + 2R\sigma_X^2 + R^2 |^3} \quad (\text{C.29})$$

$$C_{1,3} = \frac{d\sigma_X^2 (R + \sigma_X^2)^4 (R^2 + 2R\sigma_X^2 + (\alpha + 1)\sigma_X^4) \operatorname{sgn}(-((\alpha - 1)\sigma_X^4) + 2R\sigma_X^2 + R^2)}{(R^2 + 2R\sigma_X^2 - ((\alpha - 1)\sigma_X^4))^5} \quad (\text{C.30})$$

$$C_{2,1} = \begin{cases} \frac{d(R + \sigma_X^2)^3}{\alpha\sigma_X^2(-R^2 - 2R\sigma_X^2 + (\alpha - 1)\sigma_X^4)^3} (3R^2\sigma_X^2 + R^3 - 3(\alpha - 1)R\sigma_X^4 + (\alpha - 1)^2\sigma_X^6) & \text{When } R(R + 2\sigma_X^2) < (\alpha - 1)\sigma_X^4 \\ \frac{d\sigma_X^4}{(R^2 + 2R\sigma_X^2 - ((\alpha - 1)\sigma_X^4))^3} ((\alpha + 1)R^3 + 3R^2\sigma_X^2 - 3(\alpha - 1)R\sigma_X^4 + (\alpha - 1)^2\sigma_X^6) & \text{Otherwise} \end{cases} \quad (\text{C.31})$$

$$C_{2,2} = \frac{d\sigma_X^4 (R + \sigma_X^2)^4 ((\alpha + 1)R^2 - 2(\alpha - 1)R\sigma_X^2 + (\alpha - 1)^2\sigma_X^4) \operatorname{sgn}(-((\alpha - 1)\sigma_X^4) + 2R\sigma_X^2 + R^2)}{(R^2 + 2R\sigma_X^2 - ((\alpha - 1)\sigma_X^4))^5} \quad (\text{C.32})$$

$$C_{2,3} = \frac{1}{(R^2 + 2R\sigma_X^2 - ((\alpha - 1)\sigma_X^4))^7} (d\sigma_X^4 (R + \sigma_X^2)^5 ((\alpha + 1)R^4 + 3((\alpha - 2)\alpha + 2)R^2\sigma_X^4 - (\alpha - 4)R^3\sigma_X^2 + (\alpha - 4)(\alpha - 1)R\sigma_X^6 + (\alpha - 1)^2(\alpha + 1)\sigma_X^8) \operatorname{sgn}(-((\alpha - 1)\sigma_X^4) + 2R\sigma_X^2 + R^2)) \quad (\text{C.33})$$

$$C_{3,1} = \begin{cases} \frac{1}{\alpha\sigma_X^2(-R^2 - 2R\sigma_X^2 + (\alpha - 1)\sigma_X^4)^5} (d(R + \sigma_X^2)^4 ((\alpha - 1)^2(\alpha + 15)R^2\sigma_X^8 - 20(\alpha - 1)R^3\sigma_X^6 - 5(\alpha - 3)R^4\sigma_X^4 + 6R^5\sigma_X^2) & \text{When } R(R + 2\sigma_X^2) < (\alpha - 1)\sigma_X^4 \\ \frac{1}{(R^2 + 2R\sigma_X^2 - ((\alpha - 1)\sigma_X^4))^5} (d\sigma_X^6 ((\alpha(\alpha + 3) + 1)R^6 + (\alpha - 1)^2(\alpha + 15)R^2\sigma_X^8 + 4(\alpha - 1)((\alpha - 1)\alpha - 5)R^3\sigma_X^6 + (\alpha((\alpha - 12)\alpha + 6) + 15)R^4\sigma_X^4 - 2((\alpha - 5)\alpha - 3)R^5\sigma_X^2 - 6(\alpha - 1)^3R\sigma_X^{10} + (\alpha - 1)^4\sigma_X^{12})) & \text{Otherwise} \end{cases} \quad (\text{C.34})$$

$$C_{3,2} = \frac{1}{(R^2 + 2R\sigma_X^2 - ((\alpha - 1)\sigma_X^4))^7} (d\sigma_X^6 (R + \sigma_X^2)^5 ((\alpha(\alpha + 3) + 1)R^4 + 3(\alpha^3 - 3\alpha + 2)R^2\sigma_X^4 + 2(-3\alpha^2 + \alpha + 2)R^3\sigma_X^2 - 4(\alpha - 1)^3R\sigma_X^6 + (\alpha - 1)^4\sigma_X^8) \operatorname{sgn}(-\alpha\sigma_X^4 + \sigma_X^4 + 2R\sigma_X^2 + R^2)) \quad (\text{C.35})$$

$$C_{3,3} = \frac{1}{(R^2 + 2R\sigma_X^2 - ((\alpha - 1)\sigma_X^4))^9} (d\sigma_X^6 (R + \sigma_X^2)^6 ((\alpha(\alpha + 3) + 1)R^6 + 6(-\alpha^2 + \alpha + 1)R^5\sigma_X^2 + 3(\alpha - 1)^2(\alpha(2\alpha - 3) + 5)R^2\sigma_X^8 - 4(\alpha - 1)(2(\alpha - 2)\alpha + 5)R^3\sigma_X^6 + 3(\alpha(2(\alpha - 1)\alpha - 3) + 5)R^4\sigma_X^4 - 6(\alpha - 1)^3R\sigma_X^{10} + (\alpha - 1)^4(\alpha + 1)\sigma_X^{12}) \operatorname{sgn}(-\alpha\sigma_X^4 + \sigma_X^4 + 2R\sigma_X^2 + R^2)) \quad (\text{C.36})$$

Explicit expression of some of these symbols that will be required later is given below for $\alpha < 1$.

$$B_1 = \frac{dR}{R + \sigma_X^2} \quad (\text{C.37})$$

$$B_2 = \frac{dR^2}{R^2 + 2R\sigma_X^2 - \alpha\sigma_X^4 + \sigma_X^4} \quad (\text{C.38})$$

$$B_3 = \frac{dR^3 (3R^2\sigma_X^2 + R^3 + 3R\sigma_X^4 - ((\alpha^2 - 1)\sigma_X^6))}{(R^2 + 2R\sigma_X^2 - ((\alpha - 1)\sigma_X^4))^3} \quad (\text{C.39})$$

$$B_4 = \frac{1}{(R^2 + 2R\sigma_X^2 - ((\alpha - 1)\sigma_X^4))^5} (dR^4 (4(-\alpha^2 + \alpha + 5)R^3\sigma_X^6 + (\alpha((\alpha - 12)\alpha + 6) + 15)R^2\sigma_X^8 \\ + (\alpha + 15)R^4\sigma_X^4 + 6R^5\sigma_X^2 + R^6 + 2(\alpha((\alpha - 6)\alpha + 2) + 3)R\sigma_X^{10} \\ + (\alpha - 1)^2(\alpha(\alpha + 3) + 1)\sigma_X^{12})) \quad (\text{C.40})$$

$$C_{1,1} = \frac{d\sigma_X^2}{R^2 + 2R\sigma_X^2 - \alpha\sigma_X^4 + \sigma_X^4} \quad (\text{C.41})$$

$$C_{1,2} = \frac{d\sigma_X^2 (R + \sigma_X^2)^3}{(R^2 + 2R\sigma_X^2 - ((\alpha - 1)\sigma_X^4))^3} \quad (\text{C.42})$$

$$C_{1,3} = \frac{d\sigma_X^2 (R + \sigma_X^2)^4 (R^2 + 2R\sigma_X^2 + (\alpha + 1)\sigma_X^4)}{(R^2 + 2R\sigma_X^2 - ((\alpha - 1)\sigma_X^4))^5} \quad (\text{C.43})$$

$$C_{2,1} = \frac{d\sigma_X^4 ((\alpha + 1)R^3 + 3R^2\sigma_X^2 - 3(\alpha - 1)R\sigma_X^4 + (\alpha - 1)^2\sigma_X^6)}{(R^2 + 2R\sigma_X^2 - ((\alpha - 1)\sigma_X^4))^3} \quad (\text{C.44})$$

$$C_{2,2} = \frac{d\sigma_X^4 (R + \sigma_X^2)^4 ((\alpha + 1)R^2 - 2(\alpha - 1)R\sigma_X^2 + (\alpha - 1)^2\sigma_X^4)}{(R^2 + 2R\sigma_X^2 - ((\alpha - 1)\sigma_X^4))^5} \quad (\text{C.45})$$

$$C_{2,3} = \frac{d\sigma_X^4 (R + \sigma_X^2)^5}{(R^2 + 2R\sigma_X^2 - ((\alpha - 1)\sigma_X^4))^7} ((\alpha + 1)R^4 + 3((\alpha - 2)\alpha + 2)R^2\sigma_X^4 \\ - (\alpha - 4)R^3\sigma_X^2 + (\alpha - 4)(\alpha - 1)R\sigma_X^6 + (\alpha - 1)^2(\alpha + 1)\sigma_X^8) \quad (\text{C.46})$$

$$C_{3,1} = \frac{1}{(R^2 + 2R\sigma_X^2 - ((\alpha - 1)\sigma_X^4))^5} (d\sigma_X^6 ((\alpha(\alpha + 3) + 1)R^6 \\ + (\alpha - 1)^2(\alpha + 15)R^2\sigma_X^8 + 4(\alpha - 1)((\alpha - 1)\alpha - 5)R^3\sigma_X^6 \\ + (\alpha((\alpha - 12)\alpha + 6) + 15)R^4\sigma_X^4 - 2((\alpha - 5)\alpha - 3)R^5\sigma_X^2 - 6(\alpha - 1)^3R\sigma_X^{10} + (\alpha - 1)^4\sigma_X^{12})) \quad (\text{C.47})$$

$$C_{3,2} = \frac{d\sigma_X^6 (R + \sigma_X^2)^5}{(R^2 + 2R\sigma_X^2 - ((\alpha - 1)\sigma_X^4))^7} ((\alpha(\alpha + 3) + 1)R^4 + 3(\alpha^3 - 3\alpha + 2)R^2\sigma_X^4 + 2(-3\alpha^2 + \alpha + 2)R^3\sigma_X^2 - 4(\alpha - 1)^3R\sigma_X^6 + (\alpha - 1)^4\sigma_X^8) \quad (\text{C.48})$$

$$C_{3,3} = \frac{1}{(R^2 + 2R\sigma_X^2 - ((\alpha - 1)\sigma_X^4))^9} (d\sigma_X^6 (R + \sigma_X^2)^6 ((\alpha(\alpha + 3) + 1)R^6 + 6(-\alpha^2 + \alpha + 1)R^5\sigma_X^2 + 3(\alpha - 1)^2(\alpha(2\alpha - 3) + 5)R^2\sigma_X^8 - 4(\alpha - 1)(2(\alpha - 2)\alpha + 5)R^3\sigma_X^6 + 3(\alpha(2(\alpha - 1)\alpha - 3) + 5)R^4\sigma_X^4 - 6(\alpha - 1)^3R\sigma_X^{10} + (\alpha - 1)^4(\alpha + 1)\sigma_X^{12})) \quad (\text{C.49})$$

In terms of these symbols we have the following explicit formula

$$\begin{aligned} \text{Tr} \langle \hat{\Sigma}_{\theta_1} \rangle &= \alpha \Delta_T C_{1,1} + e^{2T} (B_2 - 2B_1) \\ \text{Tr} \langle \hat{\Sigma}_{\theta_1}^2 \rangle &= \alpha^2 \Delta_T^2 C_{2,2} + e^{4T} B_4 + 4e^{4T} B_2 \\ &\quad + 2\alpha \Delta_T e^{2T} \hat{R}^2 C_{1,3} - 4\alpha \Delta_T e^{2T} \hat{R} C_{1,2} - 4e^{4T} B_3 + 2\alpha \Delta_T e^{2T} C_{1,1} \end{aligned} \quad (\text{C.50})$$

As a summary our final expression for variance term in KL divergence is given by (C.10) along with (C.17), (C.22), (C.23) and (C.50). Since the expression is fairly complicated we won't present explicit formula for it. To understand the implications of the formula we look at ridgeless limit $\hat{R} \rightarrow 0$.

Putting all the results together, for $\alpha < 1$, the ridgeless formula takes the following form

$$\begin{aligned} \langle \text{KL}(\rho_G|\rho)_{\text{var}} \rangle &= \frac{1}{4} (e^{-2T} + \sigma^{-2} \Delta_T)^2 (2e^{2T} \frac{\alpha}{1-\alpha} \Delta_T d \sigma_X^{-2} + \frac{\alpha^2}{(1-\alpha)^3} \Delta_T^2 d \sigma_X^{-4}) \\ &\quad + \frac{1}{2} (e^{-2T} + \sigma^{-2} \Delta_T) (\sigma^{-2} \Delta_T e^{2T}) (\frac{\alpha}{1-\alpha} \Delta_T d \sigma_X^{-2}) + \frac{d}{4} (\sigma^{-2} e^{2T} \Delta_T)^2 \\ &= \frac{d\alpha \hat{\lambda} e^{-4T} (e^{2T} - 1)}{2(1-\alpha)} + \frac{d\hat{\lambda}^2 e^{-8T} (e^{2T} - 1)^2 (\alpha^2 + (1-\alpha)^3 e^{4T} + 4\alpha(1-\alpha)^2 e^{2T})}{4(1-\alpha)^3} \end{aligned} \quad (\text{C.51})$$

If we further consider the late time approximation we see that $\langle \text{KL}(\rho_G|\rho)_{\text{var}} \rangle \propto d\lambda^2$ to the leading order. Also note that $\langle \text{KL}(\rho_G|\rho)_{\text{var}} \rangle / d$ is an increasing function of α in this regime.

Ridgeless limit for $\alpha > 1$ is more involved and it is given by

$$\begin{aligned}
\langle \text{KL}(\rho_G|\rho)_{\text{var}} \rangle &= \frac{1}{4}(e^{-2T} + \sigma^{-2}\Delta_T)^2 \left(2e^{2T} \frac{1}{(\alpha-1)} \Delta_T d \sigma_X^{-2} + \frac{\alpha^2}{(\alpha-1)^3} \Delta_T^2 d \sigma_X^{-4} + e^{4T} d \left(1 - \frac{1}{\alpha} \right) \right) \\
&\quad + \frac{1}{2}(e^{-2T} + \sigma^{-2}\Delta_T)(\sigma^{-2}\Delta_T e^{2T}) \left(\frac{1}{\alpha-1} \Delta_T d \sigma_X^{-2} - e^{2T} d \left(1 - \frac{1}{\alpha} \right) \right) + \frac{d}{4}(\sigma^{-2}e^{2T}\Delta_T)^2 \\
&= d \frac{\alpha-1}{4\alpha} + \frac{d\hat{\lambda}e^{-4T}(e^{2T}-1)}{2(\alpha-1)} + \frac{d\hat{\lambda}^2e^{-8T}(e^{2T}-1)^2}{4(\alpha-1)^3\alpha} \\
&\quad \times (\alpha^3 + (\alpha-1)^3e^{4T} + 4\alpha(\alpha-1)^2e^{2T})
\end{aligned} \tag{C.52}$$

In this domain $\langle \text{KL}(\rho_G|\rho)_{\text{var}} \rangle/d$ is no longer a monotonic function of α . It is easy to see from the expression above that as $\alpha \rightarrow 1$ both from $\alpha > 1$ and $\alpha < 1$ side, KL divergence becomes unbounded.

Our analytical calculation can be generalized to the study a (stack of) wide neural network in the kernel approximation regime [39–46] or in mean field regime [47–50] instead of a linear diffusion model.